International Journal of Thermophysics, Vol. 23, No. 6, November 2002 (© 2002)

Thermal Conductivity Measurements of Thin Amorphous Silicon Films by Scanning Thermal Microscopy

S. Volz,[1,2] X. Feng,[3] C. Fuentes,[1] P. Guérin,[4] and M. Jaouen[4]

Received October 24, 2001

Thermal conductivity measurements of thin amorphous silicon films performed with a micro-thermistance mounted on an atomic force microscope are presented. A specific thermal model is implemented, and an identification procedure is proposed to extract the film contribution from the apparent thermal conductivity. Results show agreement with the literature regarding interface resistance data, but lower thermal conductivity values are obtained.

KEY WORDS: amorphous silicon films; interface thermal resistance; scanning thermal microscopy.

1. INTRODUCTION

With the advances in micro- and nanofabrication techniques, microelectronic and optoelectronic systems have undergone a strong enhancement through size reduction. Present-day new materials with controlled thermophysical properties [1] include micro or nanostructures, i.e., small-scale particles, wires, pores, or films. In these cases, the characteristic sizes are smaller than one micrometer so that adapted metrologies require submicrometer probes. We present thermal conductivity measurements of thin amorphous silicon films performed with a micro-thermistance mounted on

[1] École Nationale Supérieure de Mécanique et d'Aérotechnique, Laboratoire d'Études Thermiques, UMR 6608, BP 40109, 86961 Futuroscope Cedex, France.

[2] To whom correspondence should be addressed. E-mail: volz@em2c.ecp.fr

[3] Heat Transfer Laboratory, Department of Engineering Mechanics, Tsinghua University, Beijing 100084, People's Republic of China.

[4] Laboratoire de Métallurgie Physique, UMR 6630, Université de Poitiers, B.P. 179, SP2MI, 86960 Futuroscope Cedex, France.

0195-928X/02/1100-1645/0 © 2002 Plenum Publishing Corporation

an atomic force microscope (AFM). Determination of the thermal conductivity of thin films deposited on a substrate requires accounting for the interface thermal resistance and substrate contributions. This problem is not new, and identification techniques are usually based on one-dimensional models considering the contributions of the film, interface, and substrate thermal conductances [2]. This analysis fails in ultra-local characterization techniques when the probe size is of the order or smaller than the studied structure such as a submicrometer-thick thin film.

In the next section, a description of the experimental device is presented. A specific thermal model is implemented, and an identification procedure is proposed to extract the film contribution from the apparent thermal conductivity in Section 3. A discussion is provided in Section 4 on results that are consistent with literature values regarding interface resistance data. Lower thermal conductivity results compared to literature values are obtained.

2. EXPERIMENT

2.1. Apparatus Description

The probe (Topometrix®) consists of a wollaston wire shaped as a tip and etched to uncover a platinum wire core as shown in Fig. 1. The thin Pt wire with Ag contacts is mounted in a AFM device and used as a thermal element. In the thermal conductivity mode, the probe serves as a classical hot-wire anemometer: the electrical resistance R_{probe} is measured with current-voltage data and is used as an input signal for a feedback loop to

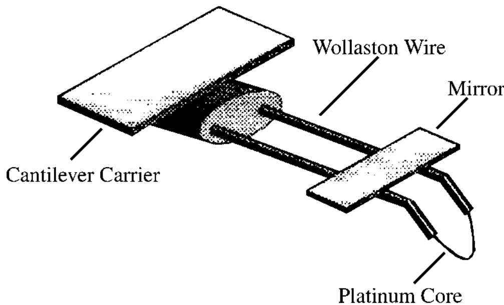

Fig. 1. Schematic of the thermal probe mounted in the atomic force microscope. The mirror allows the deflection measurement through laser reflection. The platinum core is the thermal sensitive part of the probe.

maintain the temperature which is linearly proportional to R_{probe}. The working temperature is set to $\theta_0 = 100°C$ so that water adsorbed on the sample evaporates.

The AFM system is used to control the tip position and contact force with the sample. This monitoring is performed with a feedback loop between the signals of three *x*-*y*-*z* piezo-electrical ceramics carrying the tip and four photodiodes tracking a laser beam which reflects from the probe. The probe contact force is about 1.5 μN, and the piezo scanners allow 100 μm *x*-*y* horizontal translations and 10 μm vertical displacement.

2.2. Calibration Procedure

When the probe is brought within close contact to the film surface, the induced change of the dissipated electrical power is proportional to the heat flux toward the sample and, consequently, to the sample thermal conductivity [3]. The heat flux lost in the sample can therefore be estimated at each point on the sample surface. The calibration has to be performed *in situ* since the sample/probe contact surface is small and the temperature variation of this zone will not affect the R_{probe} as would a calibration bath. The procedure simply consists of measuring the heat flux dissipated in the reference samples of well known thermal conductivity to determine the parameters of the function relating the thermal conductivity and dissipated electrical power. We assume a linear calibration function as proposed in the literature [3].

Since silicon films behave as insulators, we chose reference samples with low thermal conductivities, i.e., SiO_2 (glass-1.46 $W \cdot m^{-1} \cdot K^{-1}$) and Stirodur® (0.028 $W \cdot m^{-1} \cdot K^{-1}$). A 2% uncertainty is estimated for the electrical potential measurements, and a 4% value is therefore estimated for the precision of the electrical power data with a confidence level of 99% for the measured value to be in the range of $\pm 3\sigma$. This calibration procedure includes side effects such as the tip-sample contact conductance or radiative exchanges and conductive heat losses in the AFM tip.

2.3. Measurements

The mean value of the signal is obtained from the scanning of a 20 μm × 20 μm zone, and the contact radius of the tip is estimated to be $b = 50$ nm, with a diameter of 5 μm. 40000 points per image (1 point per 0.01 square μm) were therefore considered by fixing the image resolution. Statistical averaging was then carried out, and the accuracy range was found to be 0.001%. The high number of data points is the first reason explaining such

a high resolution. The data scatter is primarily related to the dependence of the sample/tip thermal contact resistance on the surface morphology. Figure 2 shows the scanning of bulk and rough Ag samples for which the coupling between thermal and topography signals is significant: a dip in the topography signal is related to a peak in the thermal signal. However, a low conductance sample with a clean and plane surface makes this contact resistance a less significant contribution as shown in Figs. 3(a) and (b)

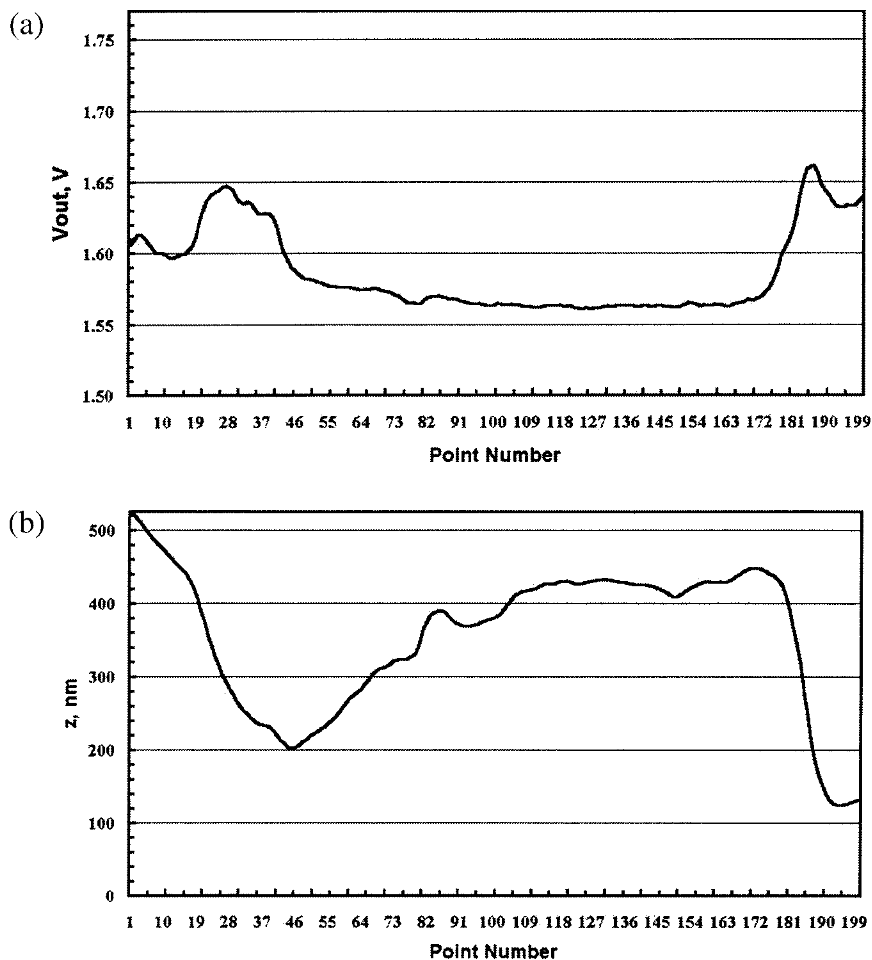

Fig. 2. (a) Thermal and (b) topography signal measured on a one line scanning. The coupling of thermal and topography due to variation of tip/sample contact surface appears clearly.

where the thermal signal of Si substrate samples can be assumed as homogeneous on the sample. The surface roughness is so small that there is no significant change in thermal conductance during the scanning. The very localized dark zones correspond to lower values for the heat flux dissipated in the sample. Those zones are removed by image processing before averaging. The obtained mean heat flux value is related to an apparent thermal conductivity by using the calibration data. Since reference samples have well controlled roughnesses, we assume that the tip/sample contact conductance is not significantly different from those for the thin film samples. We emphasize that our calibration data therefore rightly take into account the conductance parameter. The image of Fig. 3(c) reflects different conditions implying higher data scatter which is discussed in the next section.

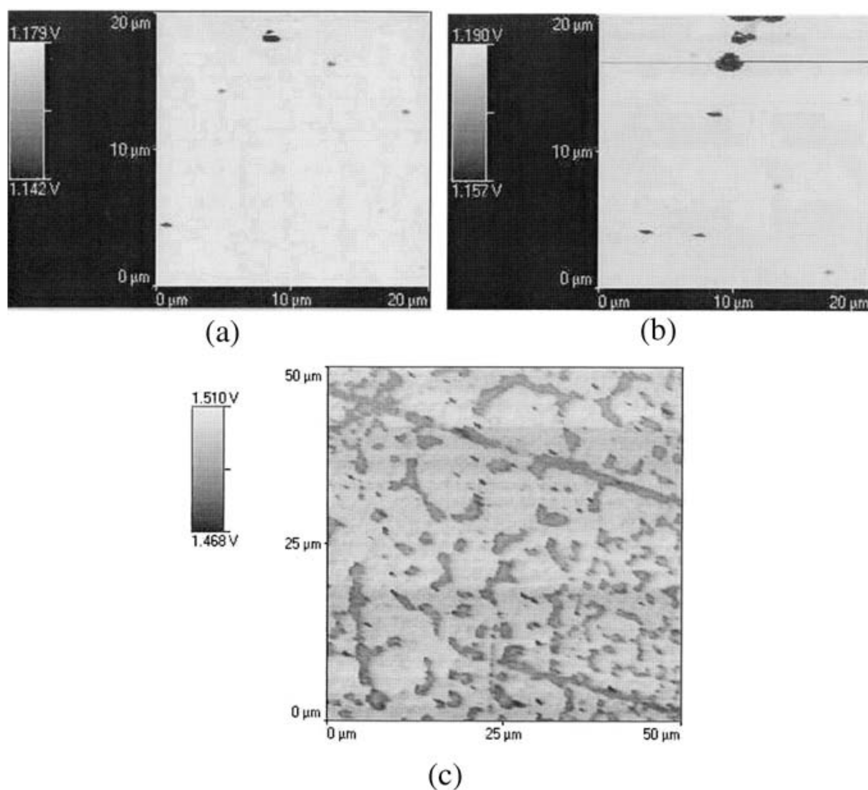

Fig. 3. Images of the thermal mapping of a 20 µm × 20 µm surface. Si substrate samples with (a) 100 nm and (b) 500 nm thick Si films. (c) Results for SiO_2 substrate with 10 nm thick Si film show islands generation: contrast between low conductive SiO_2 and Si is striking.

2.4. Samples

Three different thicknesses (10, 100, and 500 nm) of silicon films deposited on three different clean substrates (GaAs, Si, and SiO_2) were tested at room temperature. They were deposited with a sputtering beam technique that was calibrated to ensure the accuracy of the final thickness. The film thickness was also checked by atomic force microscopy on substrate/film steps generated by a mask as shown in Fig. 4(a), and a 2% uncertainty was reported. Figure 4(b) reveals that 10 nm thick films are not as smooth as thicker samples. We presume that local islands have formed during the deposition process but have not coalesced. This specific topography increases the uncertainty in the thermal measurements as mentioned concerning Fig. 3(c).

2.5. Apparent Thermal Conductivity

Figure 5 shows the thermal conductivity values obtained by using our scanning thermal probe when considering samples as bulk materials. Those apparent thermal conductivities include thin film, film/substrate and substrate conductances. These values are about two orders of magnitude lower than the thermal conductivity of monocrystalline Si (150 $W \cdot m^{-1} \cdot K^{-1}$). The thermal conductivity decrease with film thickness is clearly due to the contribution of the substrate thermal conductivity and film/substrate contact resistance as confirmed by the following three arguments:

(i) whether the silicon samples are amorphous or polycrystalline, the film conductivity should be nearly independent of thickness. A size effect only appears for large phonon mean free path (MFP) materials while amorphous Si MFP is of the order of the

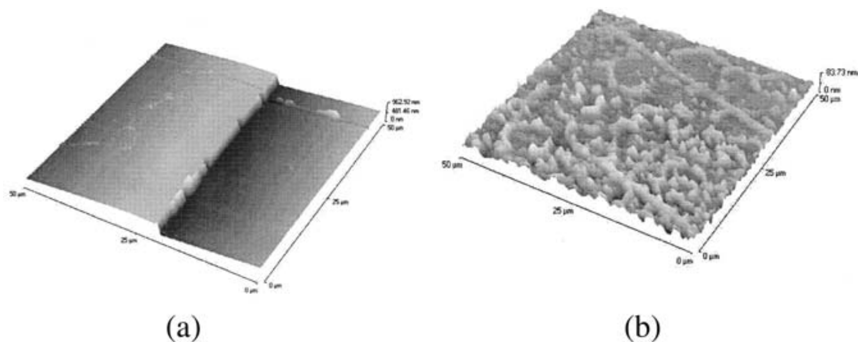

Fig. 4. Topography mapping of 500 nm thick Si film on Si substrate (a) showing the step left by the mask technique to measure the film thickness. Topography mapping of 10 nm thick Si film on SiO_2 substrate.

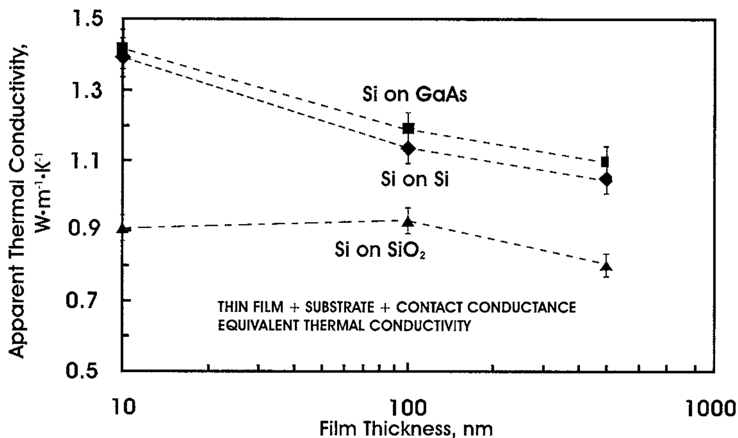

Fig. 5. Uncorrected thermal conductivity versus film thickness for the three different substrates: GaAs (squares), Si (diamonds), and SiO_2 (triangles).

interatomic distance and the polycrystalline Si MFP is limited by the grain size;

(ii) the thermal penetration depth d_{th} for which the temperature has decreased by 90% compared to the tip temperature θ_0 is defined by [4]

$$\frac{\theta(d_{th})}{\theta_0} = \left(\frac{b}{d_{th}}\right) = 0.1 \tag{1}$$

when solving the Poisson equation in spherical coordinates in a semi-infinite medium. A 0.1 value for the ratio leads to a penetration depth of 500 nm which is the maximum film thickness under test. Note that this penetration depth also provides the lateral resolution of the technique.

(iii) the SiO_2 substrate data are not strongly/remarkably affected by size because the glass conductivity is of the same order as the sample value.

It is clear that a thermal model is required to extract both the film thermal conductivity and interface resistance.

3. THERMAL MODEL AND IDENTIFICATION PROCEDURE

3.1. Thermal Model

A finite-volume method in cylindrical coordinates was implemented to model the system described in Fig. 6 consisting of the film, the interface

conductance Gc, and the substrate. A classical formalism was used, based on the assumption of fully diffusive heat transfer. An isotropic thin film thermal conductivity was assumed as a first approach and will be confirmed when proving that the film structure is amorphous. The equation to solve is the well known two-dimensional cylindrical stationary heat conduction equation:

$$\text{div}\, \boldsymbol{q}(r, z) = 0 \tag{2}$$

inside the system and the continuity relation at the substrate/film interface:

$$q(z=-t, 0<r<R) = Gc(T(-t^{+})-T(-t^{-})) \tag{3}$$

where t is the film thickness. Boundary conditions are as follows:

(i) tip/sample contact zone is approximated to a disk of radius $r_0 = b = 50$ nm and its temperature is set to the tip temperature $\theta_0 = 100\,°C$;

(ii) the adiabatic upper film surface $q_0(r > r_0) = q(r > r_0, z = 0)$ is set to zero, with q being the surface heat flux density;

(iii) the bottom surface temperature $T\ (z=-d)$ is fixed at the room temperature 20 °C;

(iv) lateral surfaces are adiabatic $q\ (r = R) = 0\ \text{W} \cdot \text{m}^{-2}$, with R being the system lateral limit.

Boundary condition (ii) is valid if the convection and radiation losses on the film surface can be neglected. This assumption will be confirmed after computing the surface temperature field by comparing heat fluxes

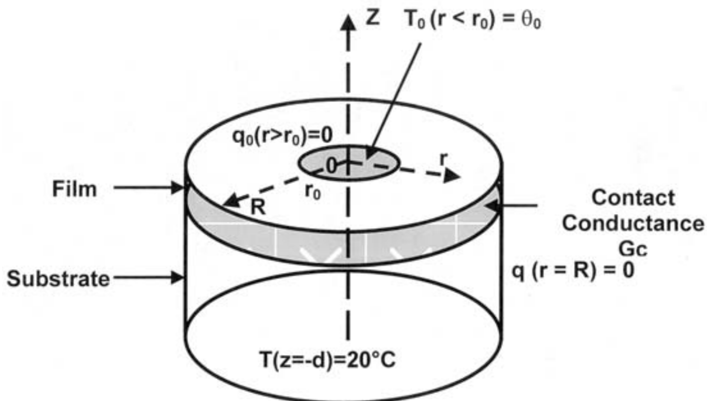

Fig. 6. Schematic of the system model based on finite volume method.

of the tip and of the remaining top surface. Conditions (iii) and (iv) are still satisfied by fixing sufficiently large $d = 1.8\ \mu m$ and $R = 0.5\ \mu m$ parameters to make the temperature rise, due to tip heating, disappear on the bottom and lateral surfaces. Substrate thermal conductivities were set to reference values provided either by the manufacturer or the literature (Si 148 $W \cdot m^{-1} \cdot K^{-1}$, SiO_2 1.4 $W \cdot m^{-1} \cdot K^{-1}$, GaAs 56 $W \cdot m^{-1} \cdot K^{-1}$).

The numerical scheme is based on the Gear predictor-corrector principle ensuring stability. Volume elements are rings with identical square sections 25 nm $\times$ 25 nm. For the 10 nm thick film, thinner elements of square sections 10 nm $\times$ 10 nm were simulated. Twenty elements were considered in the radial direction and 60 for depth. A 10 to 20 s computation time on a PC machine made the identification iteration possible.

3.2. Identification Procedure

We used the data from the 100 nm and 500 nm thick films to determine the film/substrate contact resistance Gc and the film thermal conductivity λ_f. The 10 nm thick films have non-homogeneous properties and seem therefore not reliable at this point of the analysis. The set of samples corresponding to different substrates is studied separately. Our identification procedure is as follows.

(1) First, the heat flux lost in each sample q_s is numerically estimated when the sample is assimilated to a bulk material with the experimental apparent thermal conductivity (Fig. 5). This q_s value has to be retrieved when including the realistic substrate, film thermal conductivities, and film/substrate contact conductance. We then identify both λ_f and Gc from q_s^{100} and q_s^{500} (heat flux for the 100 nm and 500 nm thick films) by using a numerical identification procedure:

(2) Given an initial value for the thermal conductivity of the 500 nm thick film, we find the Gc value leading to heat flux q_s^{500}.

(3) This conductance is then used to find the conductivity value corresponding to the heat flux q_s^{100} lost in the 100 nm thick sample. The result is input in phase 2, and the iteration is implemented.

This algorithm, if converging, will provide single λ_f and Gc values for each set of samples with same substrate.

4. RESULTS AND DISCUSSION

Figures 7(a) and (b) show the data points in a Gc versus λ_f plane at each iteration. The two distinct behaviors correspond to the progressive

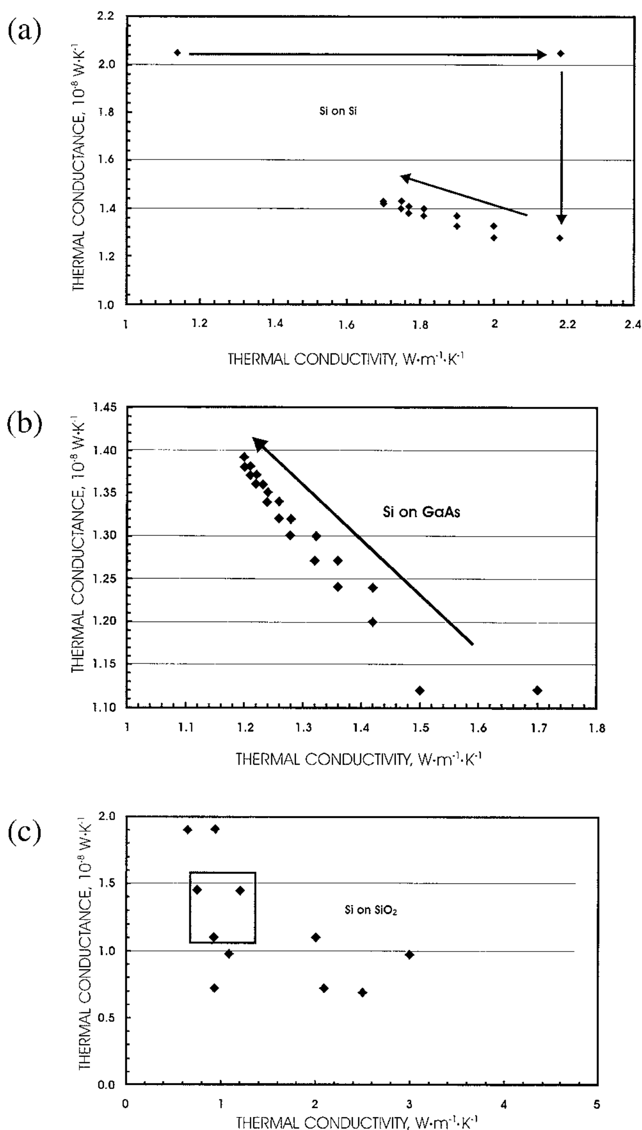

Fig. 7. Thermal conductance versus thermal conductivity results of the parameter identification method for Si (a), GaAs (b), and SiO_2 (c) substrates. Arrows show the evolution of iterations.

Table I. Thermal Conductivity and Contact Resistance for Films Grown on Si and GaAs Samples

	GaAs substrate	Si substrate
λ_f ($W \cdot m^{-1} \cdot K^{-1}$)	1.2	1.7
$Gc \times 10^8$ ($W \cdot K^{-1}$)	1.39	1.43

convergence of both 100 and 500 nm film computations. Iterations are stopped when the intersection point is obtained. Contrarily, no coherent evolution can be obtained for samples with SiO_2 substrates. In this case, the substrate and the film thermal conductivity are of the same order, and the method becomes much less sensitive to the film contribution. The black square indicates the zone where the other samples data are positioned. Final results with 10% uncertainty are reported in Table I.

Thermal conductivity values are about two orders of magnitude smaller than for bulk Si monocrystal (150 $W \cdot m^{-1} \cdot K^{-1}$). Previous studies provide information on LPCVD deposited Si films with low conductivity values. In Refs. 5 and 6, in-plane results of 15 to 23 $W \cdot m^{-1} \cdot K^{-1}$ are explained by the existence of a polycrystalline structure including Si nanocrystallites. The phonon mean free path is limited by grain size, and the heat flux is also reduced by the thermal contact resistance between crystallites. In the same studies, measurements for amorphous Si films with a mean free path of about the interatomic distance, are presented and values of about 5 $W \cdot m^{-1} \cdot K^{-1}$ are obtained. Amorphous Si films are also investigated in Ref. 7 where values ranging from 0.3 to 5 $W \cdot m^{-1} \cdot K^{-1}$ are proposed. Those data are adjusted to remove the contact resistance contribution, and a value of 5.5 $W \cdot m^{-1} \cdot K^{-1}$ is deduced.

To determine the film structure in the present study, transmission electron microscopy (TEM) experiments have been performed with a JEOL 3010 microscope operating at 300 kV. The 100 nm thick Si sample that has been used for thermal conductivity experiments was scratched with a tungsten carbide pin, and the resulting coating flakes were deposited on a holey carbon grid for the TEM observations. The edges of the flakes were thin enough to reach the electron transparency and a typical selected area diffraction (SAD) pattern is shown in Fig. 8. Such a SAD only exhibits three diffuse rings, and it proves unambiguously that the structure of the silicon film studied here is amorphous. This conclusion is supported by the fact that the deposition was realized without heating the substrate.

We assume that the differences between our thermal conductivity values and those of Refs. 5–7 can be explained by the fact that LPCVD

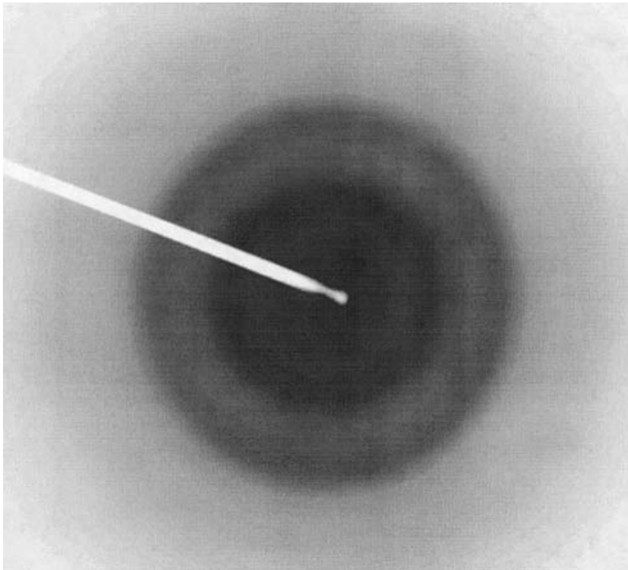

Fig. 8. Selected area diffraction (SAD) image obtained with JEOL 3010 TEM operating at 300 kV. 100 nm thick Si sample was scratched, and the resulting coating flakes were deposited on a holey carbon grid. The SAD clearly shows the amorphous structure of the Si film.

deposition techniques performed at temperatures above 500°C may still generate nanocrystallites while sputtering at ambient temperature may not. No SAD image is provided for the characterization of amorphous films structure. References 5 and 6 also target the in-plane thermal conductivity which can be expected to be higher than the cross-plane value due to anisotropic structure arrangement. Thermal conductivity data of Ref. 7 are questionable since they are deduced from a regression of seven points with a range of $\pm 20\%$ uncertainty. We however emphasize that our contact resistance values, i.e., 0.55 and 0.59 $mm^2 \cdot K \cdot W^{-1}$ for GaAs and Si substrates, respectively, are very near the value obtained by Kuo et al. [7], i.e., 0.53 $mm^2 \cdot K \cdot W^{-1}$ in the case of native-oxide covered Si substrate. The fact that the obtained contact resistances are very similar indicates that the change in the apparent thermal conductivity is mainly due to the substrate effect.

5. CONCLUSION

In conclusion, a scanning thermal microscope setup which is able to provide local thermal conductivity measurements on microscale surfaces,

was used to characterize thin Si films deposited by a sputtering technique. A calibration procedure is presented, and a thermal model including film, film/substrate contact conductance and substrate contributions is solved based on the finite volume method. Finally, a parameter identification procedure provides both thermal conductivity and film/substrate conductances. The measured low thermal conductivity values are two orders of magnitude smaller than that for the bulk monocrystal Si and two to three times smaller than data for LPCVD amorphous Si films. We presume that the different deposition technique or a large uncertainty may explain this difference.

ACKNOWLEDGMENT

The authors would like to thank the Heat Transfer Laboratory at Tsinghua University, Beijing, China, for student exchange. The support from National Natural Science Foundation of China (Grant No. 50176023) is acknowledged.

NOTE ADDED IN PROOF

The measurements performed by D. G. Cahill et al., (*J. Vac. Sci. Technol.* **A7**:1259 (1989)) together with a model considered as a reference in the field (J. L. Feldman et al., *Phys. Rev. B* **48**:12589 (1993)) provide a value of $1.28\ \mathrm{W \cdot m^{-1} \cdot K^{-1}}$ for the amorphous silicon thermal conductivity at 300 K. Those data can be considered as highly reliable and are in a much better agreement with our results: a 7% (GaAs substrate) and 39% (Si substrate) deviations are obtained. This remark strengthens the validity of our analysis and experiments in relation to those of Refs. 5–7.

REFERENCES

1. G. Chen, *Semimetals and Semiconductors, Recent Trends in Thermoelectric Materials Research III*, T. Tritt, ed., Vol. 71, pp. 203–259.
2. A. Lahmar, T. P. Nguyen, D. Sakami, S. Orain, Y. Scudeller, and F. S. O. Danes, *Thin Solid Films* **389**:167 (2001).
3. R. J. Pylkki, P. J. Moyer, and P. E. West, *Jpn. J. Appl. Phys.* **33**:3785 (1996).
4. A. Majumdar, *Ann. Rev. Mater. Sci.* **29**:505 (1999).
5. S. Uma, A. D. McConnell, M. Asheghi, K. Kurabayashi, and K. E. Goodson, *Int. J. Thermophys.* **22**:605 (2001).
6. L Wei, M. Vaudin, C. S. Hwang, G. White, J. Xu, and A. J. Steckl, *J. Mater. Res.* **10**:1889 (1995).
7. B. S. W. Kuo, J. C. M. Li, and A. W. Schmid, *Appl. Phys. A* 55:**289** (1992).